Possible ice-wedge polygonisation in Utopia Planitia, Mars and its latitudinal gradient of distribution

R. J. J Soare, Susan J. Conway, J.-P. Williams, Meven Philippe, L.E. Mc Keown, L E Mc Keown, E. Godin, J. Hawkswell

▶ **To cite this version:**

R. J. J Soare, Susan J. Conway, J.-P. Williams, Meven Philippe, L.E. Mc Keown, et al.. Possible ice-wedge polygonisation in Utopia Planitia, Mars and its latitudinal gradient of distribution. Icarus, 2021, 358, pp.114208. 10.1016/j.icarus.2020.114208 . hal-03008487v2

HAL Id: hal-03008487
https://hal.science/hal-03008487v2

Submitted on 16 Mar 2021

HAL is a multi-disciplinary open access archive for the deposit and dissemination of scientific research documents, whether they are published or not. The documents may come from teaching and research institutions in France or abroad, or from public or private research centers.

L'archive ouverte pluridisciplinaire **HAL**, est destinée au dépôt et à la diffusion de documents scientifiques de niveau recherche, publiés ou non, émanant des établissements d'enseignement et de recherche français ou étrangers, des laboratoires publics ou privés.

Possible ice-wedge polygonisation in Utopia Planitia, Mars

and

its latitudinal gradient of distribution

R.J. Soare,[1] S.J. Conway,[2] J-P Williams,[3] M. Philippe[2],
L.E. Mc Keown,[4] E. Godin[5], J. Hawkswell[6]

[1]Geography Department, Dawson College, Montreal, Qc, Canada
(rsoare@dawsoncollege.qc.ca)

[2] Laboratoire de Planétologie et Géodynamique, CNRS UMR, CNRS 6112, 2 rue de la Houssinière, 44322, Nantes, Cedex 3, France

[3]Earth, Planetary and Space Sciences, University of California, Los Angeles, CA, USA

[4]School of Natural Sciences, Trinity College Dublin, Ireland, Dublin 4, Ireland

[5]Centre for Northern Studies, Laval University, Quebec City, Qc, Canada

[6]Ocean Wise, PO Box 3232, Vancouver, BC, Canada

Pages - 38

Figures - 9

Tables - 1

Keywords - Mars, climate, surface, atmosphere

ABSTRACT

On Earth, *ice complexes* are commonplace landscapes amidst the continuous permafrost of coastal or near-coastal plains in the Arctic. Formed by the freeze-thaw cycling of water, ice complex features include: hummocky (thermokarstic) terrain, inflated or deflated by the presence of absence of excess ice; thermokarst lakes (i.e. excess ice that has thawed and pooled); alases (i.e. thermokarst basins emptied of water); and, ice-wedge polygons, often characterized by raised (ice-aggraded) or lowered (ice-degraded) margins relative to the polygon centres.

The origin and development of these complexes is rooted in inter-or intra-glacial pulses of temperature that engender widespread thaw, meltwater distribution and migration through the soil column (sometimes to decametres of depth), and the freeze-thaw cycling of the meltwater.

The possible existence of ice-rich terrain on Mars revised by the freeze-thaw cycling of water dates back to the grainy Mariner-mission photographs of the 1960s and 1970s. However, absent of regolith samples from areas where this terrain is hypothesised, attempts to validate the ice-rich hypothesis often have ended abruptly, either with spectrometric inferences of water-equivalent hydrogen to one metre or so of depth or with "looks-like", therefore "must-be" analogies derived of Earth-based ice-complexes.

In the case of small-sized Martian polygons with low- and high-centres, the similarities of form between ice and sand-wedge polygons on Earth has equivocated the reach of ice-wedge hypotheses on Mars.

Here, we show that:

1) The plains' terrain of our study region in Utopia Planitia (40-50^{o} N; 100-125^{o} E) displays a statistically-significant and positive (linear) correlation between the ratio of low-centred to high-centred polygons (*lcps* vs *hcps*) and a poleward latitude of distribution.

55 **2)** This linear correlation would be expected, in as much as ground-ice stability increases with
56 latitude, were the shoulders of higher-latitude *lcps* underlain by (aggraded) ice-wedges and
57 those of lower-latitude *hcps* underlain by (degraded) ice-wedges.
58 **3)** The change of polygon morphology with latitude would not be expected were the *lcps* and
59 *hcps* underlain by sand wedges, in as much as ground-ice stability is unrelated to their
60 aggradation or degradation.
61 **4)** Crater counts of the polygonised terrain indicate that it is less youthful than previous
62 studies have suggested, perhaps by an order of magnitude. This attenuates the possible
63 inconsistency between the more temperate boundary-conditions required by the formation
64 of ice-wedge polygons and the current constraints of extreme aridity, low temperatures and
65 low atmospheric pressure.

66 **1. Introduction**

67 On Earth, *ice complexes* (also referenced as ice-rich terrain) at or near the surface or to
68 decametres of depth are ubiquitous within the permafrost of Arctic coastal-plains, i.e. the
69 Tuktoyaktuk region of northern Canada (e.g. Rampton and Bouchard, 1975; Rampton, 1988;
70 Murton, 2005) and the Laptev peninsula of northeastern Siberia (e.g. Schirrmeister et al. 2002,
71 2017; Grosse et al. 2007; Morgenstern et al. 2013; Strauss et al. 2017). Some examples of this
72 terrain are:

73 **a)** Hummocky thermokarst (ballooned by aggraded excess-ice and deflated where the
74 excess ice has been lost by evaporation, drainage or sublimation).
75 **b)** Thermokarst lakes, i.e. pooled meltwater resulting from the thaw of excess ice.
76 **c)** Alases (thermokarst-lake basins depleted of water).

d) Ice-wedge polygons, typically ≤25 m in diameter. Morphologically, they can be distinguished by three principal archetypes. **1.** Low-centres relative to high margins/shoulders where the ice wedges have/are aggraded/aggrading; **2.** high-centres relative to low margins/troughs where the ice wedges have/are degraded/degrading; or, **3.** centres and margins that exhibit no discernable elevation difference, indicative of ice-wedge incipience or of a more mature and transitional stage between aggradation and degradation.

Pulses of ice-complex formation have been associated with inter-and intra-glacial mean-temperature rises and falls that reach back through the Holocene epoch (e.g. Rampton and Bouchard, 1975; Rampton, 1988; Murton et al. 2005; Grosse et al 2007; Morgenstern et al. 2013; Schirrmeister et al. 2013), to the Wisconsinan glacial stage (e.g. Rampton and Bouchard, 1975; Rampton, 1988; Murton et al. 2005; Grosse et al. 2007; Morgenstern et al. 2013; Schirrmeister et al. 2013) and, even into the earlier periods of the Pleistocene Epoch (e.g. Rampton, 1988; Kanevskiy et al. 2017).

Ice-wedge polygon networks are current as well as paleo-markers of temperature variances. The nascent conditions required for the ice-wedges to form are continuous permafrost, thermal-contraction cracking, meltwater, hoarfrost (to a much lesser degree), and seasonal/annual (mean) temperature fluctuations above and below 0^{o} C (e.g. Lachenbruch, 1962). Where low-centred (aggraded) and high-centred (degraded) polygons are closely set, this marks a system actively in thermal disequilibrium and transition (Washburn, 1973; French 2007; also, Rampton and Bouchard, 1975; Rampton, 1988; Schirrmeister et al. 2002; Grosse et al. 2007; Morgenstern et al. 2013).

Mars-based *lcps* and *hcps* that are similar in shape and size to those observed on Earth and, on occasion have been reported widely in the literature (e.g. Lefort et al. 2009; Levy et al. 2009a, 2010; Séjourné et al. 2011; Soare et al. 2014, 2018). Questions concerning whether ice or sand underlies the margins of the Martian *lcps* and *hcps* have been and remain open-ended, for two main reasons (e.g. Lefort et al. 2009; Levy et al. 2009a, 2010; Séjourné et al. 2011; Soare et al. 2014, 2018).

First, and based solely on the plan-based observation of *lcps* or *hcps* on Earth and on Mars, the identification or discrimination of sub-marginal materials is not possible. This is due to the similarity of form and scale between ice-and sand-wedge polygons when viewed planimetrically, from above (Levy et al. 2009a, 2010; Hallet et al. 2011; Hauber et al. 2011; Soare et al. 2014, 2018).

Second, metres-wide ice wedges are not unusual amidst northern ice-complexes on Earth. Their development is incremental and episodically iterative, ranging through hundreds of seasonal/annual freeze-thaw cycles and meltwater fills (Lachenbruch, 1962). A similar or an even greater number of iterations would be required on Mars for similarly scaled ice-wedges to evolve. Current (mean) water-vapour pressures at or near the surface are as much as two orders of magnitude lower than on Earth (e.g. Renno et al. 2013; Trokhimovskiy et al. 2015) and are inconsistent with the freeze-thaw cycling of water at a region-wide scale. There are areas, however, where the triple-point of water is exceeded (e.g. Haberle et al. 2001; Hecht, 2002). What is unclear is whether the temporal extent of this meta-stability, current, past or long past, could have supported the iterative requirements of ice-wedge formation.

In this article we plot, describe, discuss and statistically evaluate the distribution of *lcps* and *hcps* in Utopia Planitia [*UP*] (40-50^{o} N; 100-125^{o} E) **(Fig. 1)**. The latter is one of the great

northern plains of Mars. We assume that here in our study region, as elsewhere on Mars, the stability of ground ice increases with its poleward latitude. This is because (mean) annual surface and near-surface temperatures tend to remain below the atmospheric frost-point with poleward proximity, mitigating ice loss by sublimation (e.g. Clifford, 1993; Mellon and Jakosky, 1993, 1995) Consequently, ice-aggraded polygons should show a higher density of distribution with poleward proximity than ice-degraded polygons and *vice versa*.

2. Methods

All of the High Resolution Imaging Science Experiment (*HiRISE)* images (*N*=135) in our study region (40-50^{o} N; 110-125^{o} E) were surveyed for the presence of low- or high-centered polygons **(Fig. 1)**. To ensure the consistency of our observations and interpretations, multiple co-authors evaluated the images independently and our data base (**Table 1**) integrates these evaluations.

The survey itself was based on a grid-mapping approach (Ramsdale et al. 2017). Eleven images were too blurry to be evaluated; sixteen images were not surveyed because they were fully overlapped by images with higher resolution, or with equal resolution but greater spatial extent. These images have been excluded from the study and are not reported in **Table 1**. The remaining sample comprised 108 images, divided into two groups: **1)** images whose resolution and/or quality support the unambiguous identification of *lcps* and/or *hcps*, if and when they are present (67 images, of which 41 have polygons); and, **2)** images whose resolution and/or quality are of a lesser order, making the identification of *lcps* and *hcps* more difficult (41 images, of which 35 have polygons (**Table 1**).

The *HiRISE* image-footprints were gridded into reference squares of 250,000 m² (37,639 squares) **(Figs. 2a-b)**. Some squares were not fully within the *HiRISE* footprints. We excluded

four-thousand two-hundred and thirty-seven of those squares from our data base since they comprised less than half the area of a reference square, i.e. 125,000 m². A further, 111 squares were discounted because they overlapped with data gaps in the *HiRISE* image. As such, 33,291 squares were evaluated.

If five or more candidate *lcps* or *hcps* were observed within each square they were recorded. For grid squares where polygonised terrain was observed but the terrain showed neither *lcps* nor *hcps* were observed, grid squares also were noted. Where fewer than five polygons were observed of any given type, they were not recorded for that grid square; highly localized if not stochastic boundary-conditions could have been responsible for the development of these small samples and would bias our evaluation of the larger population were they to be incorporated in our statistics. We are aware of and acknowledge that our five-unit (count/no count) threshold is arbitrary, but no more so than any other small unit-threshold that could have been used to differentiate meaningful samples from meaningless ones.

For each *HiRISE* image **(Table 1)** the number grid-squares containing *lcp* data-points was divided by the number of grid-squares containing *hcp* data-points to calculate the *lcp*/*hcp* ratio of each image. Also, each scanned grid-square was related to: **a)** its centre latitude; **b)** the presence/absence of *lcps* or *hcps*; and, **c)** one of two terrain types (**Type 1** and **Type 2**) by the location of their centre point. **Type 1** comprises the whole study region exclusive of **Type 2**. The latter comprises the walls, rims and interiors of craters ≥ 2 km (in diameter). These outputs were used to evaluate the possible correlation between polygon type (i.e. the *lcp*/*hcp* ratio) and latitude/terrain type using regression analysis.

Crater counts were conducted to derive information about the age of the polygonized terrain. *HiRISE* image ESP_026450_2270 (center longitude 110.880° E, center latitude 46.823°

N) was selected within the study region as it contained polygons throughout the image; counts were conducted on the entire image covering 150 km^2 at 0.5 m pix^{-1} resolution using the *Cratertools* plug-in for the *ERSI ArcGIS* to measure crater diameters (Kneissl et al. 2011). The crater-size frequency distribution (*CSFD*) was compared with modeled crater-retention age isochrons from Hartmann (2005) using *Craterstats* (Michael and Neukum, 2010; Michael et al. 2016).

3. Observations

Small-sized (~⩽25 m in diameter) and clastically non-sorted polygons are ubiquitous in our study region. Typically, the polygons are hexagonal and enclosed by metre-scale margins. The margins exhibit: **a)** slightly-elevated (metre-high) shoulders (low-centred polygons, *lcps*) **(Figs. 3a, c)**; **b)** depressed troughs (high-centred polygons, *hcps*), relative to the polygon centres **(Figs. 3b-c)**; or, **c)** variances of elevation that are small or non-existent **(Fig. 3c)**, at the highest resolution available (~25 cm/pixel, *HiRISE* image).

Here, as elsewhere in Utopia Planitia (e.g. Costard et al. 1995; Seibert and Kargel, 2001; Morgenstern et al. 2007; Soare et al. 2007, 2008; Lefort et al. 2009; Levy et al. 2009a; Ulrich et al. 2010; Séjourné et al. 2011, 2012), the small-sized polygons show distribution at or near the surface that is wide-ranging, often covering many square kilometres **(Figs. 2a-b)**, and varied: **1)** within rimless and sometimes scalloped depressions **(Figs. 3a-c)**; **2)** amidst inter-(impact) crater plains **(Figs. 2b, 3d-e)**; and, **3)** within impact craters **(Figs. 3f-g)**. Frequently, the *lcps* are proximal to the depression margins (e.g. Lefort et al. 2009; Séjourné et al. 2011). The *hcps*, by contrast, display no similar bias.

The depressions exhibit a variety of planforms: circular (**Fig. 4a**); sub-circular or elongated (**Fig. 4b**); and, scalloped on the margins (**Fig. 4c**). Their distribution is no less varied, being

observed individually (**Fig. 4a**), clustered or coalesced (**Fig. 4c**), or in wave-like forms (**Fig. 4d**). Orientation, defined by the loss of elevation relative to the surface datum, is longitudinal and equatorward (e.g. Morgenstern et al. 2007; Lefort et al. 2009; Séjourné et al. 2011, 2012). Depths range from metres to decametres (Morgenstern et al. 2007; Lefort et al. 2009; Séjourné et al. 2011, 2012). Inward-oriented and roughly equatorial tiers or terraces often demarcate the changes of elevation and are commonplace amidst the scalloped depressions (**Fig. 4c**).

4. Ice-complex constituents on Earth

4.1 *Thermal-contraction cracking and ice wedge polygons*

In low-lying and coastal regions of ice-rich permafrost such as the Tuktoyaktuk Coastlands small-sized (generally ≤25 m in diameter), clastically non-sorted, ice-wedge polygons are observed widely (Mackay, 1974; Rampton and Bouchard, 1975; Rampton, 1988; French, 2007). Here, mean monthly-temperatures (1971-2000) range from -26.3^{o} to +10.9^{o} C, and the mean annual-precipitation, inclusive of rain and snowfall, is 139.3 cm (water equivalent) (Environment Canada, 2010).

The polygons are the product of tensile stresses in frozen soil that arise from the sharp drop of sub-zero ^{0}C temperatures (Lachenbruch, 1962). This fracturing, or thermal-contraction cracking, initially forms shallow, narrow and vertical veins **(Fig. 5a)**. The type of fill depends on the ambient boundary-conditions and the availability of: **1)** meltwater derived of thawed snow or ice; **2)** winter hoarfrost; or, **3)** windblown sand, mineral-soil, or a mixture of the two (e.g. de Leffingwell, 1915; Péwé, 1959; Lachenbruch 1962; Washburn, 1973; Sletten et al. 2003; Hallet et al. 2011).

The diurnal and seasonal iteration of cracking and filling may grow the sub-centimetre to centimetre- scale veins into wedges with metre-scale depth and width (Lachenbruch, 1962). As the cracks intercept one another they form individual polygons and, eventually, consolidated polygon

networks (Washburn, 1973; Mackay, 1974; Mackay and Matthews, 1983). The latter may comprise hundreds of square kilometres of continuous or discontinuous coverage and represent hundreds of fill and crack-formation cycles (e.g. Black, 1954; Lachenbruch, 1962; Washburn, 1973; Mackay, 1974) **(Fig. 5b)**.

Thermal-contraction polygons exhibit low **(Fig. 5c)** or high centres **(Figs. 5d-e)** relative to their margins or centres, or margins that are relatively-equal in elevation **(Fig. 5b)**, depending upon their developmental stage. Ice-wedge aggradation is informed by the (seasonally) iterative infilling and freezing of meltwater at polygon margins, as well as by the active-layer expansion that moves sediment radially to the polygon margins from the centres. This uplifts the sedimentary overburdens, forms raised shoulders (Mackay, 1981; French and Guglielmin, 2000; French, 2007) and gives the polygons a distinctly low-centred appearance (Czudek and Dumek, 1970; Rampton, 1988; Hallet et al. 2011). Ice-wedge degradation follows from a sustained rise of thaw-tolerant mean temperatures. This deflates polygon-margin shoulders, perhaps sinking them below polygon-centre elevation, morphing low-centred into high-centred polygons (Czudek and Dumek, 1970; Rampton, 1988; Hallet et al. 2011). Regions or sub-regions where *lcps* and *hcps* are observed concurrently are in thermal flux (Czudek and Dumek, 1970; Rampton, 1988; Hallet et al., 2011).

Of note; some polygon centres and their icy margins may exhibit little or no difference in their relative elevations. This either means that the ice has aggraded insufficiently to form marginal shoulders or degraded insufficiently to form marginal troughs.

4.2 Sand-wedge, composite and sublimation-enhanced polygons

Sand-wedge polygons with low and high centres are observed in relatively-temperate and ice-rich landscapes where ice-wedge polygons are present (e.g. Mackay and Matthews, 1983; Murton et al. 2000) **(Fig. 5f)**, as well as in the McMurdo Dry Valleys *(MDVs*), Antarctica, where

238 they are absent from the landscape (e.g. Péwé, 1959; Berg and Black, 1966; French and
239 Guglielmin, 2000; Marchant et al. 2002; Bockheim et al. 2002; Sletten et al. 2003; Hallett et al.
240 2011). In both cases the sand-wedge polygons are paleo-markers of climatic and hydrological
241 regimes that are drier and/or colder than those associated with the origin and development of ice-
242 wedge polygons (Washburn, 1973; Mackay and Matthews, 1983; Murton et al., 2000; Wolfe et al.
243 2018). For example, contrast the annual mean-temperatures and -precipitation at the Tuktoyaktuk
244 coastlands (discussed above) with the mean annual air-temperatures and precipitation at Beacon
245 Valley, one of the *MDVs*. At Beacon Vally, annual mean-temperatures are ~-34^{o} C and soil
246 temperatures possibly do not exceed ~0^{o} C (Marchant et al., 2002). Precipitation is meagre
247 (<50mm of water equivalent precipitation per annum) and is comprised solely of snowfall
248 (Bockheim et al. 2002; Levy 2015). Boundary conditions consistent with the iterative formation
249 of ice-wedge polygons are rare, perhaps not exceeding a few days per annum.

250 Sand-wedge polygons originate and develop by the same thermal stresses that engender
251 the formation of ice-wedge polygons (e.g. Berg and Black, 1966; Péwé, 1959; French and
252 Gugliemin, 2000; Marchant et al. 2002; Sletten et al. 2003; Hallet et al. 2011). Morphologically,
253 the rise and fall of polygon margins follows a slightly different path. The latter deform upwardly,
254 forming (raised shoulders) *lcps*, as sand and other surface minerals accumulate by the work of
255 wind; downward deformation, i.e. the transformation of raised shoulders into marginal troughs, by
256 aeolian erosion, creates *hcps* (e.g. Péwé, 1959; French and Gugliemin, 2000; Marchant et al. 2002;
257 Sletten et al. 2003; Hallet et al. 2011). Sometimes, the evolution of *hcps* is enhanced or accelerated
258 by the sublimation of underlying glacial ice (Marchant et al. 2002).

259 *4.3 Thermokarst and ice-rich landscapes*

Thermokarst refers to landforms developed by way of freeze-thaw cycling in permafrost composed of excess ice (e.g. Taber, 1930; Penner, 1959; Hussey, 1966; Hughes, 1974; Rampton, 1973, 1988; Harris et al. 1988; Osterkamp et al. 2009). Excess ice = "…the volume of ice in the ground that exceeds the total pore volume that the ground would have under unfrozen conditions" (e.g. Harris et al. 1988; also, see Taber, 1930; Penner, 1959; Rampton and Mackay, 1971; Washburn, 1973; Murton, 1996; Rampton, 1988; French, 2007).

Excess ice comprises ice lenses, veins, wedges or larger masses of consolidated ice that are formed by ice segregation. Fine to medium-grained soils such as silts or silty clays are particularly adept at hosting segregation ice because they have relatively-small interstices (Taber, 1930; Black, 1954; Penner, 1959; Rampton and Mackay, 1971; Rampton, 1988; Sone at al. 2006; French, 2007; Abramov et al., 2008). Small interstices facilitate the migration of pore water to and the formation of discrete layers or lenses of segregation ice at the freezing front (Taber, 1930; Penner, 1959; Rampton and Mackay, 1971; Rampton, 1988; French, 2007). Were the grain-size too fine, pore-water migration would be overly constricted and ice lenses would not form; were the grain-size too coarse, pore-water migration would be overly expeditious and flush out of the system before segregation ice could form.

Where excess ice aggrades, frost heave follows (Taber, 1930; Penner, 1959; Rampton, 1988). Where excess ice thaws and degrades, the terrain subsides and settles under its own weight, until it reaches a consolidated state (Harris et al., 1988) **(Figs. 6a-b)**. If thaw-generated meltwater pools then a thermokarst pond or lake forms; were the pooled meltwater to be lost by evaporation or drainage, an emptied basin or alas would form (Washburn, 1973; Rampton, 1988; French, 2007). Were the loss of pooled water partial and episodic, inwardly-oriented benches or terraces

may develop on the alas margins; this imparts to the margins a distinctly-scalloped appearance (e.g. Brown et al. 1981; Soare et al. 2008, 2011).

Spatially, the dense or sparse distribution of heaved and subsided terrain, as well as of thermokarst lakes and alases, in ice-rich terrain delineates two things: **1)** the breadth and scale of thermal flux and disequilibrium in that region (e.g. Péwe, 1954; French, 2007; Grosse et al. 2007; Schirrmeister et al. 2013; Wetterich et al. 2014); and, **2)** a measure of the volumetric loss of ice in that region (e.g. Czudek and Demek, 1970; Rampton and Mackay, 1971; Washburn, 1973, Rampton, 1988; French, 2007). This is no less true of ice-rich landscapes where *lcps* and hcps are observed concurrently.

5. Results

5.1 LCPs/HCPs and poleward latitude **(Table 1)**

All of the possible *lcps* or *hcps*, regardless of the group of the image they are located in (i.e. **1.** images whose resolution/quality allows unambiguous identification of polygons; and, **2.** images whose lower resolution/quality make the identification of polygons more uncertain), show similar changes of morphology with their poleward latitude. As such, both datasets are combined in the following results. We identified 313 squares with *lcps* and no *hcps*, 3,325 squares with *hcps* and no *lcps*, 663 squares with both *lcps* and *hcps*, and 10,349 squares with flat polygons, generating a total of 14,650 polygonised grid-squares (**Table S1**). The study area (40-50°N, 100-125°E) comprised 23,380 grid squares classified as terrain **Type 1** and 9,911 classified as terrain **Type 2 (Table S1)**.

Overall, the ratio of low to high-centered polygons does not show any correlation with increasing latitude (R^2 ~0.0143) **(Fig. 7)**, despite the frequency of polygonised squares increasing with latitude. However, when we excluded polygons in **Type 2** terrain from the sample data, a

statistically-significant linear correlation appears between the *lcp*-to-*hcp* ratio and latitude (R^2 > 0.87, *p-value* <0.05 (**Fig. 8**). Note that **Fig. 8** and **Table S1** data include three latitudinal ranges without *lcps* (40°-<41°, 42°-<43°, 43°-<44°; *lcp/hcp* = 0), and one range without polygons (41°-<42°; *lcp/hcp* = no data).

Crater interiors (**Type 2**) host lower temperatures and slightly-higher atmospheric-pressures than the exterior terrain populated by them; these cold traps enhance the stability and preservation of volatiles (e.g. Conway et al. 2012; also, Ingersoll et al. 1992; Dickson et al. 2010). Low-centred ice-wedge polygons, formed under antecedent boundary conditions consistent with the freeze-thaw cycling of water but cold-trapped by recent or current conditions, would be able to survive and avoid degradation at much lower latitudes than similar polygons exposed to greater variances of temperature and pressure in the surrounding inter-crater terrain **(Type 1)**. Excluding the crater-based polygons in **Type 2** terrain from our regression analysis prevents our results from being biased by these geographical outliers.

Sixty-eight percent of the squares with *lcps* also have *hcps*. This increases to 83% if **Type 2** grid squares are excluded from the count and decreases to 37% when **Type 2** grid-squares alone are counted.

5.2 Surface-age estimates

Crater counts conducted on the polygonized terrain in our study region provide information about the surface age. A total of 168 craters were identified in a 150 km^2 area of the polygonised terrain in *HiRISE* image ESP_026450_2270 (**Fig. 9**). The crater-size frequency distribution (*CSFD*) of the crater population has a much shallower power-law slope than predicted by production functions (e.g. Hartmann, 2005) and thus does not represent a formation age, but rather a “crater retention age” regulated by a destruction rate that in general preferentially removes

smaller craters (e.g. Öpik 1965; Hartmann 1971; Smith et al. 2008; Kite and Mayer 2017; Williams et al., 2018; Palucis et al. 2020).

The emplacement of these terrain materials and other mid-latitude mantling deposits has been suggested to have occurred very late in martian history as a consequence of recent climate excursions based on a general paucity of craters observed in lower-resolution MOC images (e.g. Head et al., 2003; Morgenstern et al. 2007). However, more recent observations of craters on the polygonized terrains within *UP* using higher-resolution HiRISE images, suggests a more complicated history. Craters with a fresh appearance, unmodified by polygon formation, were used by Levy et al. (2009a; 2009b) to estimate a minimum age for the cessation of emplacement of mantling material ~1.5 Ma at this latitude (~45°) and *CSFDs* on polygonised terrain measured by Soare et al. (2020) suggested a more protracted history of emplacement and modification for the polygonised materials in *UP* with a modelled surface exposure age at least ~100 Ma.

The number of craters $D > 50$ m in our count area suggests the material was emplaced and exposed to impact cratering for at least 10 Myrs, possibly longer, and precludes a surface as young as the most recent obliquity variations (Laskar et al., 2004). The CSFD suggests the surface has experienced substantial degradation. This is supported by the morphologies of the craters in various states of degradation; many of them exhibit shallow hollows. Moreover, this demonstrates that the polygonised surface has undergone erosion, the likely agent responsible for the removal of many of the craters in a size-dependent manner (e.g. Hartmann, 1971; Smith et al. 2008; Williams et al. 2018).

6. A geochronology of periglaciation at the mid-latitudes of Utopia Planitia

Here, we present an integrated geochronology that comprises a baseline of generally-accepted ideas and reasoning within the community complemented by our own observations, deductions and statistical findings.

6.1 The origin and development of ice-rich terrain

Stage 1a: Atmospheric water-vapour (the Martian equivalent of winter hoar-frost on Earth) diffuses and charges the pore space of near-surface regolith (top few metres) with ice at all latitudes during one or more periods of high obliquity during the Late Amazonian Epoch (e.g. Clifford, 1993; Mellon and Jakosky, 1993, 1995; Douglas and Mellon, 2019). In concert (or not) with this diffusion-driven ice-charging of near-surface regolith, high obliquities engender enhanced periods of H_2O-ice precipitation. The latter accumulates at the surface and forms an icy mantle (e.g. Head et al. 2003; Forget et al. 2006; Madeleine et al. 2009, 2014).

Stage 1b: Sub-aerial temperatures sufficient to host the freeze-thaw cycling of the icy mantle and near-surface regolith occur, perhaps for a few hours per sol at the appropriate solar longitude (Rivera-Valentin et al. 2020) but through sufficient annual iterations for excess ice and ice-wedge polygons to form (Soare et al. 2014, 2017, 2018). The presence of brine-bearing sediments could/would have facilitated the onset and iteration of this process because salt depresses the freezing point of water (e.g. Brass 1980; Fairén et al. 2008; Rennó et al., 2009; Möhlmann and Thomsen, 2011; Martinez et al., 2013; Travis et al. 2013; Toner and Catling, 2018; Rivera-Valentin et al. 2020). The recent work of Rivera-Valentin et al. (2020) points to brines possibly being present today in our study region.

Further facilitation could have been provided, as is the case in ice-rich permafrost regions on Earth, by the presence of relatively fine-to medium-grained regolith (Soare et al., 2015; based on: Taber, 1930; Black, 1954; Penner, 1959; Rampton and Mackay, 1971; Rampton, 1988; Sone

372 at al. 2006; French, 2007; Abramov et al., 2008). The latter would have been delivered to our study
373 region by aeolian (Bristow and Moller, 2018) or volcanic surface processes (Hoppington and
374 Leverington, 2014).

375 **Stage 2:** As high obliquity/ies wanes/wane, near-surface ground ice at the lower mid-
376 latitudes of our study region loses stability and sublimates (Mellon and Jakosky, 1993, 1995).
377 Thermokarst or alas-like basins form where the volatile loss occurs (Morgenstern et al. 2007;
378 Lefort et al. 2009; Ulrich et al. 2010; Séjourné et al., 2011, 2012; Mangold, 2011; Soare et al.
379 2014; Dundas et al. 2015; Dundas, 2017). The episodic or intermittent return to higher obliquities,
380 much like glacial inter-stades on Earth (e.g. Rampton and Bouchard, 1975; Rampton, 1988),
381 could/would have replenished and recharged the volatile-depleted terrain with ice. Against this
382 backdrop, the rimless and sometimes scalloped depressions in our study region, and throughout
383 the mid-latitudes of *UP* might be indicative of the net loss of ice-richness through the Late
384 Amazonian Epoch to the present day. Their shape, size, depth, and location possibly reflect random
385 differences in the distribution and depth of ground ice as well as in the reach of thermal
386 disequilibrium (Soare et al. 2018). In this regard, the inwardly-oriented steps or tiers often
387 observed within the depressions could be markers of an episodic loss of ice, much in the same way
388 as tiered thermokarst basins in the Tuktoyaktuk region point to the episodic loss of water (Soare
389 et al. 2007, 2008; 2017; also, Séjourné et al. 2011, 2012).

390 *6.2 The origin and development of ice-wedge polygons*

391 **Stage 3:** As we suggested in **Section 5.2**, thermal-contraction cracking polygonises the
392 terrain within the depressions, perhaps 100 Mya. Additionally, we propose that thaw-derived
393 meltwater is produced, whenever local/regional boundary conditions are fitting, with the possible
394 assistance of near-surface brines, and maybe in conjunction with higher obliquities. The meltwater

fills the polygonised cracks episodically. As the ice aggrades the regolith margins rise above the elevation datum of the polygon centres. This forms low-centred polygons (Séjourné et al. 2011, 2012; Soare et al. 2014; 2018). As earlier, recharge by the atmospheric diffusion of water vapour could be of assistance in maintaining the volume and structural integrity of the ice wedges (Clifford, 1993; Mellon and Jakosky, 1993, 1995).

Later and lower obliquities, whereby the stability of ground ice falls, sublimate/degrade the ice-wedges preferentially at lower latitudes. This transforms high-shouldered margins into low-shouldered troughs, revises *lcps* into *hcps*, and decreases the ratio of *lcps* to *hcps* at these latitudes. Sand-wedge polygons would not be expected to fit the pattern of latitudinal distribution associated with the *lcps* and presented in **Section 5.1**, nor would the linear correlation between the *lcp/hcp* ratio and poleward latitudes.

Stage 4a: In conjunction with more recent high-obliquities a metres-deep icy and lightly-toned dusty mantle(s) accumulates in our study region (e.g. Mustard et al. 2001; Head et al. 2003; Forget et al. 2006; Madeleine et al. 2009). The mantle buries or mutes the thermokarstic (polygonised) depressions and the polygonised terrain incised by the depressions (Soare et al. 2017).

Stage 4b: As Mars moved cyclically back to lower obliquity(ies) the surface mantle began to sublimate and erode, uncovering and exhuming the terrain populated by the thermokarst-like depressions and possible ice-wedge polygons (Soare et al. 2017). Mirroring the antecedent and pre-mantling losses of ice, polygons at the lower latitudes show a higher observed-distribution of low shoulders or troughs (*hcps*) than polygons at higher latitudes.

7. Discussion & Conclusion

7.1 What if…

418 Questions concerning the possible existence of ice-rich terrain on Mars date back to the
419 grainy Mariner-mission photographs of the 1960s and 1970s (e.g. Belcher et al. 1971; Sharp et al.
420 1971). In the aftermath, data-based validation of this hypothesis has been fleeting. "Looks-like"
421 therefore "must-be" inferences of thermokarst-like landforms or of possible ice-wedge polygons
422 are suggestive, even beguiling, but inadequate.

423 Validation, however, requires ground-truth, i.e. direct evidence of near-surface ground ice
424 by a human or a robotic shovel at the latitudes of our study or, possibly, a *GPR* operating at
425 frequencies sufficient to identify discrete and heterogeneous emplacements of ground ice from the
426 near-surface to depth. Current inferences of widespread water-equivalent hydrogen (possible near-
427 surface ground-ice) derived from orbital spectrometry have been less than satisfying. The data
428 have a relatively short/shallow skin-depth ($\leq$ 1 m) and a kilometre-scale footprint (e.g. Boynton et
429 al. 2002; Feldman et al. 2002, 2004; Mitrofanov et al. 2002).

430 More recent observations of Utopia Planitia (~70-90^{o} E), slightly to the west of our study
431 region and derived of the ShallowRadar (*SHARAD*, Mars Reconnaissance Orbiter), point to the
432 possible presence of a large and near-surface but decametres-deep body of admixtured ice, air and
433 dust (Stuurman et al. 2016). Whether this buried body comprises massive ice, excess ice or
434 something else remains open-ended, as does the time-frame of its origin, i.e. late Noachian Epoch,
435 early or mid-Amazonian Epochs, etc, and the process by which it came to be, i.e. glacial, fluvial,
436 marine, periglacial, a combination thereof, or something else.

437 North of our study region and substantially to the east (68.22^{o} N, 234.30^{o} E), shallow
438 trenches dug by the Phoenix Lander revealed patches of light-toned ice that could be the work of
439 ice/soil segregation (Mellon et al. 2009). The light-toned near-surface ice is thought to be
440 geologically young, perhaps no older than 100 kyr (Mellon et al. 2009), much younger than the

441 periglacial terrain discussed by us above. The depth and distribution of this segregated ice, at this
442 location and possibly elsewhere, is unknown.

443 *7.2 Poleward latitude, ice-wedging and the freeze-thaw cycling of water*

444 **1)** Our study region in Utopia Planitia (40-50^{o} N; 100-125^{o} E) displays a statistically-
445 significant and positive (linear) correlation between the ratio of low-centred to high-centred
446 polygons (*lcps* vs *hcps*) and a poleward gradient of *lcp/hcp* distribution. As near-surface
447 ground ice is more stable at higher latitudes than at lower ones, the increased (observed)
448 occurrence of *lcps* at poleward latitudes would be expected were their margins underlain
449 by ice-wedges. Also expected would be the lower prevalence of *lcps* at the equatorward
450 latitudes where ice is less stable than at poleward ones.

451 **2)** This latitudinal gradient of *lcp/hcp* distribution would not be expected or predicted were
452 the polygon margins underlain by sand wedges. The gains and losses of elevation in the
453 margins of sand-wedge polygons are driven by aeolian accumulation or erosion or, in
454 relatively unique periglacial contexts, by the sublimation of underlying glacial-ice.
455 Variances in the stability of ground-ice, expressed on a local, regional or latitudinal scale,
456 exercise no positive or negative effect on the relative elevations of sand-wedge polygon
457 centres or margins.

458 **3)** The morphometric/statistical validation of ice-wedge polygonization along a latitudinal
459 gradient of distribution at the mid-latitudes of *UP* accomplishes two things. First, it
460 enhances the empirical/observational depth of excess-ice hypotheses and, second, it
461 underpins the possibility that excess-ice could be present, even today, at lower than
462 poleward (Phoenix-like) latitudes and closer to the surface in the northern plains than might
463 otherwise be thought.

464 **4)** Equally important is a return to questions concerning the time-scale required to form metre-
465 high ice-wedges on Mars. Ice-wedges on Earth may originate and evolve into mature
466 landforms on relatively short scales of time. For example, within a few years of a
467 thermokarst lake in the Tuktoyaktuk region having been drained of its water artificially,
468 the newly-exposed basin underwent permafrost aggradation; thermal-contraction cracking
469 also was observed, as were nascent ice-wedges (Mackay and Burn, 2002). Although
470 hundreds of seasonal/annual freeze-thaw cycles are required to evolve mature and metre-
471 scale ice wedges from sub-centimetre ice veins, even this somewhat extended period is
472 relatively short, geologically speaking.

473 On Mars, the areas where liquid water is meta-stable today could have been much
474 more long-standing and wide-ranging in the past under more favourable obliquity
475 solutions, especially if surface or near surface brines were present then as they appear to
476 be now. This would have depressed the freezing point of water and lowered the temperature
477 constraints on its freeze-thaw cycling.

478 **5)** The crater counts (see **Section 5.2**) of the polygonised terrain in our region indicate that
479 the latter is substantially older than previous studies of similar terrain in Utopia Planitia
480 have suggested, perhaps by an order of magnitude. This attenuates the possible
481 inconsistency between the more temperate boundary-conditions required by the formation
482 of ice-wedge polygons, under higher obliquities perhaps, and the current constraints of
483 extreme aridity, low temperatures and low atmospheric-pressure. Additionally, slightly-
484 higher temperatures in a volatile-rich environment could have induced an accompanying
485 rise of atmospheric vapour-pressure. This would have shortened the period of time and the
486 number of iterative (freeze-thaw) cycles required to originate and grow ice wedges.

487 **6)** Attention also ought to be cast on the possibility that disparate transformational-processes
488 might be responsible for ice-wedge aggradation and ice-wedge degradation on Mars. The
489 freeze-thaw cycling of water may be the most plausible means by which wedge ice, or even
490 segregation ice, aggrade, on Mars as on Earth. On the other hand, the degradation of
491 Martian wedge or segregation ice could and most probably is the work of sublimation.
492 Reconciling the two end-processes may be no more difficult than ascribing a less than
493 recent origin or aggradation period to the ice wedges and a possibly very-late Amazonian
494 Epoch and much more recent degradation period to them.

495 **Acknowledgements**

496 We thank the two anonymous reviewers whose comments, suggested edits and thought-provoking
497 ideas enabled us to improve this article substantially. *SJC* is grateful for the support of her *HiRISE*
498 related work by the French Space Agency (*CNES*). The contributions by *JPW* were supported by
499 the *NASA* Solar System Workings grant 80NSSC18K0010. The work of *MP* was supported by the
500 Agence Nationale de la Recherche (*ANR*) project ANR-19-CE01-0010 PERMOLARDS.

501 **References**

502 Abramov, A., Gruber, S., Gilchinsky, D. 2008. Mountain permafrost on active volcanoes: field
503 data and statistical mapping; Klyuchevskaya volcano group, Kamchatka, Russia.
504 Permafrost and Periglacial Processes 19, 261-277. doi.org/10.1002/ppp.622.

505 Belcher, D., Veverka, J., Sagan. C. 1971. Mariner photography of Mars and aerial photography
506 of Earth: some analogies. Icarus 15, 241-252.

507 Berg, T.E., Black, R.F. 1966. Preliminary measurements of growth of nonsorted polygons,

508 Victoria Land, Antarctica. In: Tedrow, J.C.F. (Ed.), Antarctic Soils and Soil-forming
509 Processes Antarctic Research Series 8. American Geophysical Union, Washington, DC,
510 pp. 61-108.
511 Bockheim, J.G., Hall, K.J. 2002. Permafrost, active-layer dynamics and periglacial environments
512 of continental Antarctica. South African Journal of Science 98, 82-90.
513 Boynton, W.V. et al. 2002. Distribution of hydrogen in the near-surface of Mars: evidence for
514 subsurface ice deposits. Science 297, 81, doi:10.1126/science.1073722.
515 Brass, G.W. 1980. Stability of brines on Mars. Icarus 42, 20-28, doi.org/10.1016/0019-1035(80)
516 90237-7.
517 Bristow, C.S., Moller, T.H. 2018. Dust Production by Abrasion of Eolian Basalt Sands: Analogue
518 for Martian Dust. Journal of Geophysical Research, doi.org/10.1029/2018JE005682.
519 Brown, R.J.E., Johnston, G.H., Mackay, J.R., Morgenstern, N.R., Shilts, W.W. 1981. Chapter 2:
520 Permafrost distribution and terrain characteristics, 31-72, in G.H. Johnson, (ed.),
521 Permafrost Engineering, Design and Construction. Associate Committee on Geotechnical
522 Research, National Research Council of Canada, John Wiley & Sons, Toronto, 540 p.
523 Clifford, S.M. 1993. A Model for the Hydrologic and Climatic Behavior of Water on Mars.
524 Journal of Geophysical Research 98, E6, 10,973-11,016.
525 Conway, S.J., Hovius, N., Barnie, T., Besserer, J., Le Mouélic, S., Orosei, R., Read, N.A. 2012.
526 Climate-driven deposition of water ice and the formation of mounds in craters in Mars'
527 north polar region. Icarus 220, 174-193, dx.doi.org/10.1016/j.icarus.2012.04.021.
528 Costard, F.M., Kargel J.S. 1995. Outwash plains and thermokarst on Mars. Icarus 114, 1, 93-
529 112, doi.10.1006/icar.1995.1046.
530 Czudek, T., Demek, J. 1970. Thermokarst in Siberia and its influence on the development of

lowland relief. Quaternary Research 1, 103-120.

De K. Leffingwell, E. 1915. The dominant form of ground-ice on the north coast of Alaska. The Journal of Geology 23, 7, 635-654.

Dickson, J.L., Head, J.W., Marchant, D.R. 2010. Kilometer-thick ice accumulation and glaciation in the northern mid-latitudes of Mars: Evidence for crater-filling events in the Late Amazonian at the Phlegra Montes. Earth and Planetary Science Letters 294, 332-342, doi:10.1016/j.epsl.2009.08.031.

Dundas, C.M., Byrne, S., McEwen, A.S. 2015. Modeling the development of Martian sublimation thermokarst landforms. Icarus 262, 154-169, doi.org/10.1016/j.icarus.2015.07.033.

Dundas, C.M. 2017. Effects of varying obliquity on Martian sublimation thermokarst landforms. Icarus 281, 1, 115-120, doi.org/10.1016/j.icarus.2016.08.031.

Environment Canada (2010). Canadian Climate Normals, 1981 - 2010. Tuktoyaktuk, http://climate.weather.gc.ca/climate_normals/index_e.html.

Fairén, A.G, Davila, A.F., Gago-Duport, L., Amils, R., McKay, C.P. 2009. Stability against freezing of aqueous solutions on early Mars. Nature 459, 401-404, doi.org/10.1038/nature 07978.

Feldman, W.C. et al. 2002. Global Distribution of Neutrons from Mars: Results from Mars Odyssey. Science 297, 75, doi:10.1126/science.1073541.

Feldman, W.C. et al. 2004. Global distribution of near-surface hydrogen on Mars. Journal of Geophysical Research 109, E09006, doi:10.1029/2003JE002160.

Forget, F., Haberle, R.M., Montmessin, D., Levrard, B., Head, J.W. 2006. Formation of glaciers on Mars by atmospheric precipitation at high obliquity. Science 311, 368, doi.10.1126/ science/1120335.

554 French, H.M. 2007. The periglacial environment, 3rd ed., J. Wiley & Sons, West Sussex, England,
555 458 p.
556 French, H.M., Guglielmin, M. 2000. Frozen ground phenomena in the vicinity of Terra Nova Bay,
557 northern Victoria Land, Antarctica: a preliminary report. Geografiska Annaler 82, A, 513-
558 526.
559 Grosse, G., Schirrmeister, L., Siegert, C., Kunitsky, V.K., Slagoda, E.A., Andreev, A.A.,
560 Dereviagyn, Y. 2007. Geological and geomorphological evolution of a sedimentary
561 periglacial landscape in northeast Siberia during the late Quaternary. Geomorphology 86,
562 25-51, doi.10.1016/j.geomorph.2006.08.005.
563 Haberle, R.M, McKay, C.P., Schaeffer, J., Cabrol, N.A., Grin, E.A., Zent, A.P., Quinn, R. 2001.
564 On the possibility of liquid water on present-day Mars. Journal of Geophysical Research
565 106, E10, 23,317-23,326.
566 Hallet, B., Sletten, R., Whilden, K. 2011. Micro-relief development in polygonal patterned ground
567 in the Dry Valleys of Antarctica. Quaternary Research 75, 347-355, dx.doi.org/10.1016/j.
568 yqres.2010.12.009.
569 Harris, S.A., French, H.M., Heginbottom, J.A., Johnston, G.H., Ladanyi, B., Sego, D.C., van
570 Everdingen, R.O. (eds.), 1988. Glossary of permafrost and related ground-ice terms.
571 Technical Memorandum 142, Permafrost Subcommittee, National Research Council of
572 Canada, 154 p.
573 Hartmann W.K. 1971. Martian cratering III: Theory of crater obliteration. Icarus 15, 410-428,
574 doi.org/10.1016/0019-1035(71)90119-9.
575 Hartmann, W.K. 2005. Martian cratering 8: Isochron refinement and the chronology of Mars.
576 Icarus 174, 294-320, doi.org/10.1016/j.icarus.2004.11.023.

577 Hauber, E. et al. 2011. Periglacial landscapes on Svalbard: Terrestrial analogs for cold-climate
578 landforms on Mars, in Geological Society of America Special Papers 483, 177-201,
579 doi:10.1130/2011.2483(12).
580 Head, J.W., Mustard, J.F., Kreslavsky, M.A., Milliken, R.E., Marchant, D.R. 2003. Recent ice
581 ages on Mars. Nature 426, 797-802, doi.10.1038/nature02114.
582 Hecht, M.H. 2002. Metastability of liquid water on Mars. Icarus 176, 373-386.
583 Hopper, J.P., Leverington, D.W. 2014. Formation of Hrad Vallis (Mars) by low viscosity lava
584 flows. Geomorphology, 207, 96-113, dx.doi.org/10.1016/j.geomorph.2013.10.029.
585 Ingersoll, A.P., Svitek, T., Murrray, B.C. 1992. Stability of Polar Frosts in Spherical Bowl-Shaped
586 Craters of the Moon, Mercury, and Mars. Icarus 100, 40-47.
587 Kanevskiy, M., Shur, Y., Fortie, D., Jorgenson, M.T., 2011. Cryostratigraphy of late Pleistocene
588 syngenetic permafrost (yedoma) in northern Alaska, Itkillik River exposure. Quaternary
589 research 75.3: 584-596, doi.org/ 10.1016/j.yqres.2010.12.003
590 Kite E.S., Mayer D.P. 2017. Mars sedimentary rock erosion rates constrained using crater counts,
591 with applications to organic-matter preservation and to the global dust cycle. Icarus 286,
592 212-222, doi.org/10.1016/j.icarus.2016.10.010.
593 Kneissl, T., van Gasselt, S., Neukum, G. 2011. Map-projection-independent crater size-frequency
594 determination in GIS environments - new software tool for ArcGIS. Planetary and Space
595 Science 59, 1243–1254, doi.org/10.1016/j.pss.2010.03.015.
596 Lachenbruch, A.H. 1962. Mechanics of Thermal Contraction Cracks and Ice-wedge Polygons in
597 Permafrost. GSA Special Paper 70. vol. 69 Geological Society of America, New York.

598 Laskar, J., Correia, A.C.M., Gastineau, M., Joutel, F., Levrard, B., Robutel, P. 2004. Long term
599 evolution and chaotic diffusion of the insolation quantities of Mars. Icarus 170, 343-364,
600 doi.org/10.1016/j.icarus.2004.04.005.
601 Lefort, A., Russell, P.S., McEwen, A.S., Dundas, C.M., Kirk, R.L. 2009. Observations of
602 periglacial landforms in Utopia Planitia with the High Resolution Imaging Science
603 Experiment (*HiRISE*). Journal of Geophysical Research 114, E04005, doi.10.1029/
604 2008JE003264.
605 Levy, J.S. 2015. A hydrological continuum in permafrost environments: The morphological
606 signatures of melt-driven hydrology on Earth and Mars. Geomorphology 240, 70-82,
607 doi.org/10.1016/j.geomorph.2014.02.033.
608 Levy, J.S, Head, J.W., Marchant, D.R. 2009a. Thermal contraction crack polygons on Mars:
609 Classification, distribution, and climate implications from HiRISE observations. Journal of
610 Geophysical Research 114, E01007, doi:10.1029/2008JE003273.
611 Levy, J.S, Head, J.W., Marchant, D.R. 2009b. Concentric crater fill in Utopia Planitia: History and
612 interaction between glacial “brain terrain” and periglacial mantle processes. Icarus 202,
613 462-476, doi.org/10.1016/j.icarus.2009.02.018.
614 Levy, J.S, Marchant, D.R., Head, J.W. 2010. Thermal contraction crack polygons on Mars. A
615 synthesis from HiRISE, Phoenix and terrestrial analog studies. Icarus 206, 229-252,
616 doi.org/10. 1016/j.icarus.2009.09.005.
617 Mackay, J.R. 1974. Ice wedge cracks, Garry Island, Northwest Territories. Canadian Journal of
618 Earth Sciences 11, 1366-1383.
619 Mackay, J.R. 1980. Deformation of ice-wedge polygons, Garry Island, Northwest Territories.
620 Geological Survey of Canada 80, 1A, 287-291.

621 Mackay, J.R. 1981. Active layer slope movement in a continuous permafrost environment, Garry
622 Island, Northwest Territories, Canada. Canadian Journal of Earth Science 18, 1666-1680.
623 Mackay, J.R, Burn, C.R. 2002. The first 20 years (1978–1979 to 1998–1999) of ice-wedge growth
624 at the Illisarvik experimental drained lake site, western Arctic coast, Canada. Canadian
625 Journal of Earth Science 39, 95-111, doi:10.1139/E01-048.
626 Mackay, J.R., Matthews, J.V. 1983. Pleistocene ice and sand wedges, Hooper Island, Northwest
627 Territories. Canadian Journal of Earth Sciences 20, 1087-1098.
628 Madeleine, J-B., Forget, F., Head, J.W., Levrard, B., Montmessin, F., Millour, E. 2009.
629 Amazonian northern mid-latitude glaciation on Mars: a proposed climate scenario. Icarus
630 203, 390-405, doi.org/10.1016/j.icarus.2009.04.037.
631 Madeleine, J-B. et al. 2014. Recent ice ages on Mars: the role of radiatively active clouds and
632 cloud microphysics. Geophysical Research Letters 41, 14, 4873-4879, doi.10.1002/2014G
633 L059861.
634 Mangold, N. 2011. Ice sublimation as a geomorphic process: a planetary perspective.
635 Geomorphology 126, 1-17. doi.1016/j.geomorph.2010.11.009.
636 Marchant, D.R. et al. 2002. Formation of patterned ground and sublimation till over Miocene
637 glacier ice in Beacon Valley, southern Victoria Land, Antarctica. Geological Society of
638 America Bulletin 114, 6, 718-730.
639 Martínez, G.M., Renno. N.O. 2013. Water and brines on Mars: current evidence and implications
640 for MSL. Space Science Reviews 175, 1-4, 29–51, doi.org/10.1007/s11214-012-9956-3.
641 Mellon, M.T., Jakosky, B.M. 1993. Geographic Variations in the Thermal and Diffusive Stability
642 of Ground Ice on Mars. Journal of Geophysical Research 98, E2, 3345-3364.
643 Mellon, M.T., Jakosky, B.M. 1995. The distribution and stability of ground ice during past and

644 present epochs. Journal of Geophysical Research 100, E6, 11,781-11799.
645 Mellon, M.T. et al. 2009. Ground ice at the Phoenix Landing Site: Stability state and origin. Journal
646 of Geophysical Research 114, E00E07, doi:10.1029/2009JE003417.
647 Michael, G.G., Neukum, G. 2010. Planetary surface dating from crater size-frequency distribution
648 measurements: partial resurfacing events and statistical age uncertainty. Earth and
649 Planetary Science Letters 294, 223-229. doi.org/10.1016/j.epsl.2009.12.041.
650 Michael G.G., Kneissl T., Neesemann, A. 2016. Planetary surface dating from crater size-
651 frequency distribution measurements: Poisson timing analysis. Icarus 277, 279-285,
652 doi.org/10.1016/j.icarus.2016.05.019.
653 Mitrofanov et al. 2002. Maps of Subsurface Hydrogen from the High Energy Neutron Detector,
654 Mars Odyssey. 297, 78-81, doi:10.1126/science.1073616.
655 Möhlmann, D., Thomsen, K. 2011. Properties of cryobrines on Mars. Icarus 212, 1, 123-130,
656 doi.org/10.1016/j.icarus.2010.11.025.
657 Morgenstern, A., Hauber, E., Reiss, D., van Gasselt, S., Grosse, G., Schirrmeister, L. 2007.
658 Deposition and degradation of a volatile-rich layer in Utopia Planitia, and implications for
659 climate history on Mars. Journal of Geophysical Research 112, E06010, doi.10.1029/
660 2006JE002869.
661 Morgenstern, A., Ulrich, M., Günther, F., Roessler, S., Fedorova, I.V., Rudaya, N.A., Wetterich,
662 S., Boike, J., Schirrmeister, L. 2013. Evolution of thermokarst in east Siberian ice-rich
663 permafrost: a case study. Geomorphology 201, 363–379, doi.org/10.1016/j.geomorph.
664 2013.07.011.
665 Murton, J.B. 1996. Thermokarst-lake basin sediments, Tuktoykatuk Coastlands, western arctic
666 Canada. Sedimentology 43, 737-760.

667 Murton, J.B. 2001. Thermokarst sediments and sedimentary structures, Tuktoyaktuk Coastlands,
668 western Arctic Canada. Global and Planetary Change 28, 175-192.
669 Murton, J.B., Whiteman, C.A., Wallier, R.I., Pollard, W.H., Clark, I.D., Dallimore, S.R. 2005.
670 Basal ice facies and supraglacial melt-out till of the Laurentide Ice Sheet, Tuktoyaktuk
671 Coastlands, western Arctic Canada. Quaternary Science Reviews 24, 681-208.
672 Murton, J.B., Worsley, P., Gozdsik, J. 2000. Sand veins and wedges in cold aeolian environments.
673 Quaternary Science Reviews 19, 899-922.
674 Mustard, J.F., Cooper, C.D., Rifkin, M.R. 2001. Evidence for recent climate change on Mars
675 from the identification of youthful near-surface ground ice. Nature 412, 411-414, doi.10.
676 1038/35086515.
677 Öpik E.J. 1965. Mariner IV and craters on Mars. Irish Astronomical Journal ,7, 92-104.
678 Palucis, M.C., Jasper, J., Garczynski, B., Dietrich, W.E. 2020. Quantitative assessment of
679 uncertainties in modeled crater retention ages on Mars. Icarus, 341, 113623, doi.org/10.
680 1016/j.icarus.2020.113623.
681 Penner, E. 1959. The mechanism of frost heaving in soils. Highway Research Board, Bulletin
682 225, 1-22.
683 Péwé, T. 1959. Sand-wedge polygons (tessellations) in the McMurdo Sound region, Antarctica-
684 a progress report. American Journal of Science 257, 545-552.
685 Rampton, V.N. 1988. Quaternary geology of the Tuktoyaktuk Coastlands, Northwest Territories,
686 Geological Survey of Canada, Memoir 423, 98 p.
687 Rampton, V.N., Bouchard, M. 1975. Surficial geology of Tuktoyaktuk, district of Mackenzie.
688 In: Geological Survey of Canada, Paper 74-53, 17 p.
689 Rampton, V.N. Mackay, J.R. 1971. Massive ice and icy sediments throughout the Tuktoyaktuk

690 Peninsula, Richards Island, and nearby areas, District of Mackenzie, Geological Survey of
691 Canada, Paper 71-21, 16 p.
692 Ramsdale, J., et al. 2017. Grid-based mapping: A method for rapidly determining the spatial
693 distributions of small features over very large areas. Planetary and Space Science 140, 49-
694 61, dx.doi.org/10.1016/j.pss.2017.04.002.
695 Rennó, N. O. et al. 2009. Possible physical and thermodynamical evidence for liquid water at the
696 Phoenix landing site. Journal of Geophysical Research 114, E00E03, doi:10.1029/2009JE
697 003362.
698 Rivera-Valentín, E.G., Chevrier, V.F., Soto., A. Martínez, G. 2020. Distribution and habitability
699 of (meta)stable brines on present-day Mars. Nature Astronomy, doi.org.10.1038/s41550-
700 020-1080-9.
701 Schirrmeister, L., Siegert, C., Kunitzky, V.V., Grootes, P.B., Erlenkeuser, H. 2002. Late
702 Quaternary ice-rich permafrost sequences as a paleoenvironmental archive for the Laptev
703 Sea Region in northern Siberia. International Journal of Earth Sciences 91, 154-167, doi.
704 10.1007/s005310100205.
705 Schirrmeister, L. Froese, D., Tumskoy, V., Grosse, G., Wetterich, S. 2013. Yedoma: late
706 Pleistocene ice-rich syngenetic permafrost of Beringia. S.A. Elias & C.J. Mock, (eds.),
707 Encyclopedia of Quaternary Science 2nd ed., 3, 542-552.
708 Schirrmeister et al. 2017. Yedoma Ice Complex of the Buor Khaya Peninsula (southern Laptev
709 Sea). Biogeosciences 14, 1261–1283, doi.org/10.5194/bg-14-1261-201.
710 Schorghofer, N., Forget, F. 2012. History and anatomy of subsurface ice on Mars. Icarus 220,
711 1112-1120, doi.10.1016/j.icarus.2012.07.003
712 Seibert, N.M., Kargel, J.S. 2001. Small-scale Martian polygonal terrain: implications for liquid

713 surface water. Geophysical Research Letters 28, 5, 899-902.
714 Séjourné, A., Costard, F., Gargani, J., Soare, R.J., Fedorov, A., Marmo, C. 2011. Scalloped
715 depressions and small-sized polygons in western Utopia Planitia: a new formation
716 hypothesis. Planetary and Space Science 59, 412-422, doi:10.1016/j.pss.2011.01.007.
717 Séjourné, A., Costard, F., Gargani, J., Soare, R.J., Marmo, C. 2012. Evidence of an eolian ice-rich
718 and stratified permafrost in Utopia Planitia, Mars. Planetary and Space Science 60, 284-
719 254, doi.10.1016/j.pss.2011.09.004.
720 Sharp, R.P., Soderblom, L.A., Murray, B.C., Cutts, J.A. 1971. The surface of Mars: 2. Uncratered
721 terrains. Journal of Geophysical Research 76, 2, 331-342.
722 Sletten, R.S., Hallet, B., Fletcher, R.C. 2003. Resurfacing time of terrestrial surfaces by the
723 formation and maturation of polygonal patterned ground. Journal of Geophysical Research
724 108, E4, 8044, doi.org/10.1029/2002JE001914.
725 Smith, M.R., Gillespie, A.R., Montgomery, D.R. 2008. Effect of obliteration on crater-count
726 chronologies for Martian surfaces. Geophysical Research Letters 35: L10202,
727 doi.org/10.1029/2008GL033538.
728 Soare, R.J., Conway, S.J., Dohm, J.M. 2014. Possible ice-wedge polygons and recent landscape
729 modification by “wet” periglacial processes in and around the Argyre impact basin, Mars.
730 Icarus 233, 214-228, doi.org/10.1016/j.icarus.2014.01.034.
731 Soare, R.J., Conway, S.J., Gallagher, C., Dohm, J.M. 2017. “Ice-rich” (periglacial) vs “icy”
732 (glacial) depressions in the Argyre region, Mars: a proposed cold-climate dichotomy of
733 landforms. Icarus 282, 70-83, doi.10.1016/j.icarus.2016.09.009.
734 Soare, R.J., Conway, S.J., Gallagher, C.J., Williams, J-P., Osinski, G.R. 2018. Paleo-periglacial

735 and “ice-rich” complexes in Utopia Planitia, Chapter 7, in, Dynamic Mars, recent
736 landscape evolution of the red planet, eds. Soare, R.J., Conway, S.J. and Clifford, S.M.,
737 Elsevier, 464 p.
738 Soare, R.J., Conway, S.J., Williams, J-P, Gallagher, C., Mc Keown, L.E. 2020. Possible (closed
739 system) pingo and ice-wedge/thermokarst complexes at the mid latitudes of Utopia
740 Planitia, Mars. Icarus 342, 113233, doi.org/10.1016/j.icarus.2019.03.010.
741 Soare, R.J., Horgan, B., Conway, S.J., Souness, C., El-Maarry, M.R. 2015. Volcanic terrain and
742 the possible periglacial formation of “excess ice” at the mid-latitudes of Utopia Planitia,
743 Mars. Earth and Planetary Science Letters 423, 182-192, dx.doi.org/10.1016/j.epsl.2015.
744 04.033.
745 Soare, R.J., Kargel, J.S., Osinski, G.R., Costard, F. 2007. Thermokarst processes and the origin
746 of crater-wall gullies in Utopia and western Elysium Planitia. Icarus 191, 1, 195-750 212,
747 doi.org/10.1016/j.icarus.2007.04.018.
748 Soare, R.J., Osinski, G.R., Roehm, C.L. 2008. Thermokarst lakes and ponds on Mars in the very
749 recent (late Amazonian) past. Earth and Planetary Science Letters 272, 1-2, 382-393, doi.
750 10.1016/j.epsl.2008.05.10.
751 Soare, R.J., Séjourné, A., Pearce, G., Costard, F., Osinski, G.R. 2011. The Tuktoyaktuk coastlands
752 of northern Canada: a possible “wet” periglacial analogue of Utopia Planitia, Mars.
753 Geological Society of America 483, 203-218, doi.org/10.1130/2011.2483(13).
754 Sone, T., Yamagata, K., Otsuki, Y., Sawada, Y., Vyatkina, M. 2006. Distribution of permafrost
755 on the west slope of Mt. Ichinsky, Kamchatka, Russia. Bulletin of Glaciological Research.
756 23, 69-75.
757 Strauss, J. et al. 2017. Deep Yedoma permafrost: A synthesis of depositional characteristics and

758 carbon vulnerability. Earth Science Reviews 172, 75-86, doi.org/10.1016/j.earscirev.2017.
759 07.007.
760 Stuurman, C.M., Osinski, G.R., Holt, J.W., Levy, J.S., Brothers, T.C., Kerrigan, M., Campbell,
761 B.A. 2016. SHARAD detection and characterization of subsurface water ice deposits in
762 Utopia Planitia, Mars, Geophysical. Research Letters, 43, doi:10.1002/2016GL070138.
763 Taber, S. 1930. The mechanics of frost heaving, 9-26, in Historical perspectives in frost heave
764 research: the early works of S. Taber and G. Beskow. Special report 91-23, U.S. Army
765 Corp of Engineers, (eds.) P.B Black and M.J. Hardenburg, 1991, 159 p.
766 Toner, J.D., Catling, T.C. 2018. Chlorate brines on Mars: Implications for the occurrence of liquid
767 water and deliquescence. Earth and Planetary Science Letters 497, 161-168, doi.org/10.
768 1016/j.epsl.2018.06.011.
769 Travis, B.J., Feldman, W.C., Sylvestre, M. 2013. A mechanism for bringing ice and brines to the
770 near surface of Mars. Journal of Geophysical Research 118, 877-890,
771 doi:10.1002/jgre.20074, 2013.
772 Trokhimovskiy, A., Fedorova, A., Korablev, O., Montmessin, F., Bertaux, J-L., Rodin, A., Smith,
773 M.D. 2015. Mars' water vapor mapping by the SPICAM IR spectrometer: Five martian
774 years of observations. Icarus 251, 50-64,
775 Ulrich, M., Morgenstern, A., Günther, F., Reiss, D., Bauch, K.E., Hauber, E., Rössler, S,
776 Schirrmeister, L. 2010. Thermokarst in Siberian ice-rich permafrost: comparison to
777 asymmetric scalloped depressions on Mars. Journal of Geophysical Research 115, E10009,
778 doi:10.1029/2010JE003640.
779 Washburn, A.L. 1973. Periglacial Processes and Environment. St Martin's Press, New York, NY,
780 pp. 320.

781 Wetterich et al. 2014. Ice complex formation in arctic East Siberia during the MIS3 Interstadial
782 Quaternary Science Reviews 84, 39-55, dx.doi.org/10.1016/j.quascirev.2013.11.009.
783 Williams, J.-P., Bogert, C.H., Pathare, A.V., Michael, G.G., Kirchoff, M.R., Hiesinger, H. 2018.
784 Dating very young planetary surfaces from crater statistics: a review of issues and
785 challenges. Meteoritic and Planetary Sciences 53, 554-582, doi.org/10.1111/maps.12924.
786 Wolfe, S.A., Morse, P.D., Neudorf, C.M., Kokelj, S.V., Lian, O.L., O'Neill, H.B. 2018.
787 Contemporary sand wedge development in seasonally frozen ground and paleo-
788 environmental implications. Geomorphology 308, 215-229, doi.org/10.1016/j.geomorph.
789 2018.02.015.

790 **Figures**

791 **Fig 1.** View of the study region in Utopia Planitia (Lambert conformal conic-projection). The
792 footprints of the 119 *HiRISE* images scanned for this study displayed with different colours
793 according to the type(s) of polygons observed therein: blue, low-centred polygons (*lcps*);
794 red, high-centred polygons (*hcps*); blue/red strips: *lcps* and *hcps*; white: no polygons; and,
795 black: non-analysable image. Background: *MOLA* (Mars Orbiter Laser Altimeter)
796 elevation data overlapping *THEMIS* (Thermal Emission Imaging System) daytime-*IR*
797 mosaics. *MOLA* data credit: *MOLA* Science Team; Arizona State University; *THEMIS*
798 image credit: Arizona State University.

799 **Fig. 2. a)** *HiRISE* image ESP_055038_2250 gridded by 500x500 metres squares (background:
800 *MOLA* elevation data overlapping a *THEMIS* daytime-*IR* mosaic). **b)** Zoom on four
801 500x500 metres-squares that illustrate the mapping method. Red and blue dots respectively
802 locate *lcps* and *hcps*. North is up on all tiles. *HiRISE* image credit: *NASA*/*JPL*/University

of Arizona; *MOLA* data credit: *MOLA* Science Team; Arizona State University; *THEMIS* image credit: Arizona State University.

Fig. 3. Examples of the three polygon-types, categorised by the relative elevation-differences between polygon centres and margins, and disparate locations, in our study region. **a)** Scalloped depressions overprinted completely by *lcps* (*HiRISE* image PSP_006908_2215, 41.178° N, 124.130° E, 25cm/pixel). **b)** Ubiquitous distribution of *hcps* throughout scalloped terrain (*HiRISE* image ESP_046467_2280, 47.594° N, 119.679° E, 25cm/pixel). **c)** Proximal *lcps* (black arrows) and *hcps* (white arrows) (*HiRISE* image ESP_055038_2250, 44.757° N, 113.888° E, 50cm/pixel). **d)** Polygons with no observable elevation-difference between centres and margins (*HiRISE* image ESP_026450_2270, 46.823º N, 110.880º E, 50cm/pixel). **e)** Larger-scale view of panel **d)** within the inter-crater plains. **f)** *Lcps* (black arrows) and *hcps* (white arrows) in close proximity (*HiRISE* image ESP_036366_2235, 42.939º N, 115.428º E, 50cm/pixel). **g)** Panel **f)** at a larger scale. Note: these polygons are in **Type 2** terrain (background: *THEMIS* day-*IR* controlled mosaic). North is up in all images. *HiRISE i*mage credits: *NASA*/*JPL*/University of Arizona.

Fig 4. a) Circular and individual rimless depressions *(HiRISE* image ESP_053205_2235, 43.350° N, 117.223° E, 25cm/pixel). **b)** Elongated rimless-depression *(HiRISE* image ESP_026094_2250, 44.657° N, 111.415° E, 25cm/pixel). **c)** Coalesced rimless depressions; note the scalloping of margins *(HiRISE* image ESP_026094_2250, 44.657° N, 111.415° E, 25cm/pixel). Note the inward-facing tiers (black dashed lines). **d)** Wave-like depressions (*HiRISE* image ESP_035667_2295, 49.377° N, 115.622° E, 25cm/pixel). North is up on all tiles. *HiRISE* image credits: *NASA*/*JPL*/University of Arizona.

Fig. 5. a) Early-stage polygonization of continuous permafrost, by way of thermal contraction

826 cracking (Tuktoyaktuk, Northwest Territories, Canada). **b)** Ubiquitous coverage of
827 continuous permafrost by small-sized, possibly ice-wedge, polygons (Husky Lakes, [*HL*]
828 midway between Tuktoyaktuk and Inuvik, Northwest Territories). **c)** Low-centred (ice-
829 wedge) polygons, with marginal but elevated troughs hosting wedge-derived meltwater
830 (*HL*). **d)** High-centred (ice-wedge) polygons, with marginal troughs filled with melt-water
831 (*HL*). **e)** Ice-wedge exposure in scarp eroded by Beaufort Sea wave-action (Peninsula
832 Point, ~6 km southwest of Tuktoyaktuk, Northwest Territories, Canada). Note the surface
833 depressions above the large ice-wedge on the right and the dangling ice-wedge remnants
834 to its left. The depressions, were they observed planimetrically, would comprise the
835 marginal troughs of high-centred (degradational) polygons. The brownish sediments in
836 whose midst the ice-wedges lie are silty clays. **f)** Exposed sand wedge (Tuktoyaktuk
837 Coastlands) (Murton et al., 2000). Image credits for all panels other than **f)**: R. Soare.
838 **Fig. 6. a)** Hummocky thermokarst, featuring thermokarst lakes, polygonised alases and beaded
839 streams linking thaw pools of degraded ice-wedge polygons (Husky Lakes, Northwest
840 Territories). **b)** Panoramic and cross-sectional view of an ice complex comprised of ice
841 wedges (on the right-hand side) and massive ice. The small, surface depressions flanking
842 the largest ice wedge (on the right-hand side, black arrows) mark the location of bilateral
843 polygonal troughs associated with a field of high-centered polygons. In a wet permafrost-
844 environment high-centered, ice-wedge polygons form when and if local or regional (mean)
845 temperatures rise to the point of inducing thaw and melt at or near the surface where the
846 ice wedges occur. Grayish-beige material on the right and throughout the floor of the
847 terrace comprises silts and clays that have slumped to the floor from the near surface as
848 retrogressive thaw has eroded this Beaufort Sea headland. The oblong block on the right-

hand side of the terrace floor points to the recentness of thaw-based detachment as there is a gap in the overhang of the terrain immediately above the block location (Peninsula Point, Northwest Territories). Image credits: R. Soare.

Fig. 7. Low-centred vs high-centred polygon latitudinal ratios for all terrain types. Data for all images have been binned for each degree of latitude excluding the upper bound. The black dashed line represents the linear correlation between *lcp*/*hcp* and latitude, its R^2 value specified above it. No correlation is observable. Error bars are calculated by assuming one in 15 squares could be erroneously classified and are not visible if they fall within the points.

Fig. 8. Low-centred vs high-centred polygon latitudinal ratios (plains, excluding craters). Data for all images have been binned for each degree of latitude excluding the upper bound. The black dashed line represents the linear correlation between *lcps*/*hcps* and latitude. The R^2 value is specified above it. A significant correlation is observed (*p-value*: 6.65×10^{-5}). Error bars are calculated by assuming one in 15 squares could be erroneously classified and are not visible if they fall within the points.

Fig. 9. a) Portion of *HiRISE* image ESP_026450_2270 within the study region (centered on 46.823° N, 110.880° E) showing impact craters on the polygonized terrain. **b)** Cumulative unbinned and **c)** log-incremental root-2 binned crater size-frequency distribution for the entire *HiRISE* image (Area: 150 km^2) with absolute model age isochrons for 1 Ma, 10 Ma, and 100 Ma surfaces shown from Hartmann (2005). *HiRISE* image credit: *NASA*/*JPL*/University of Arizona.

Fig. 1

Click here to access/download;Figure;Fig. 1.tif

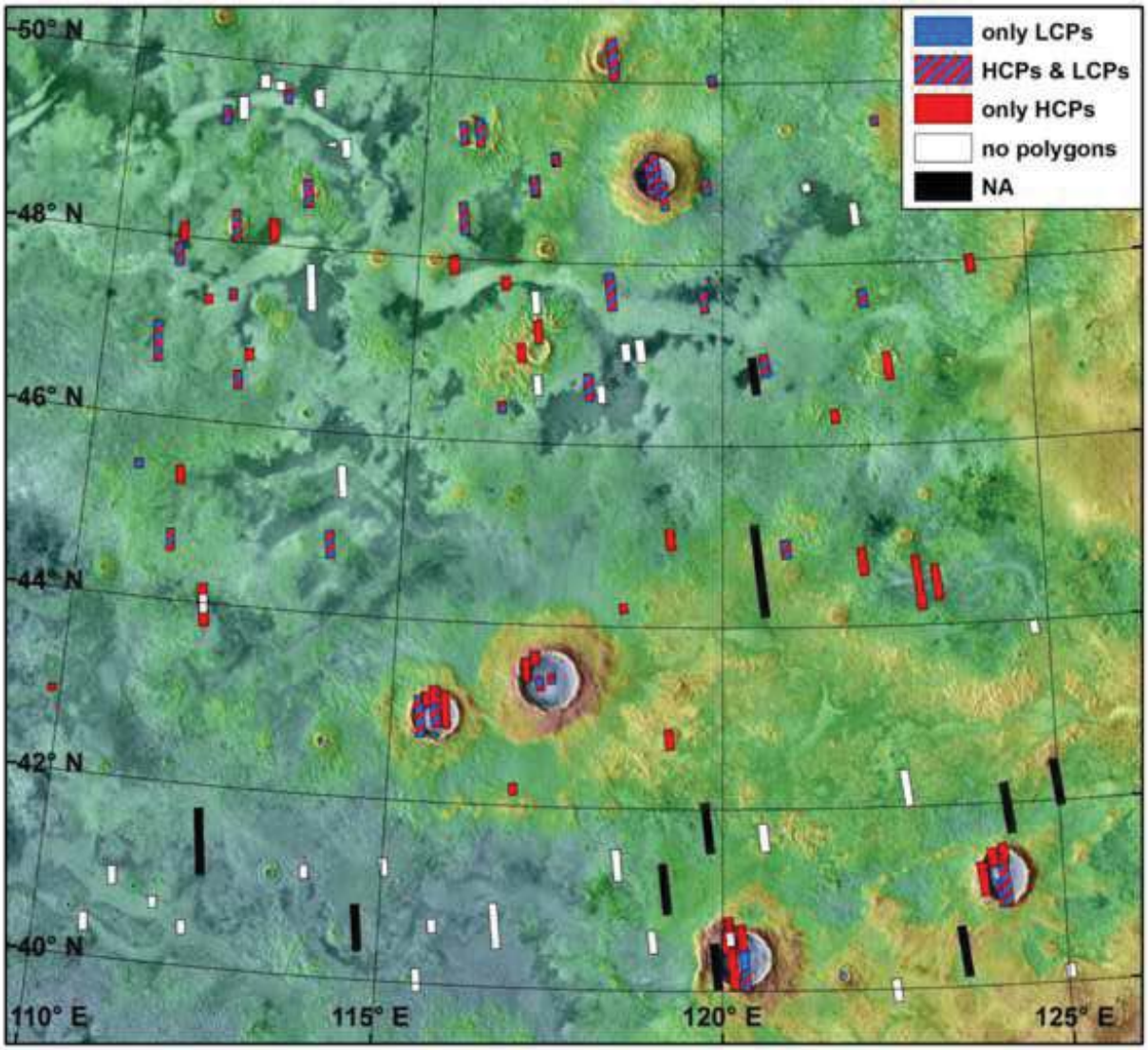

Fig. 2

Click here to access/download;Figure;Fig. 2.jpg

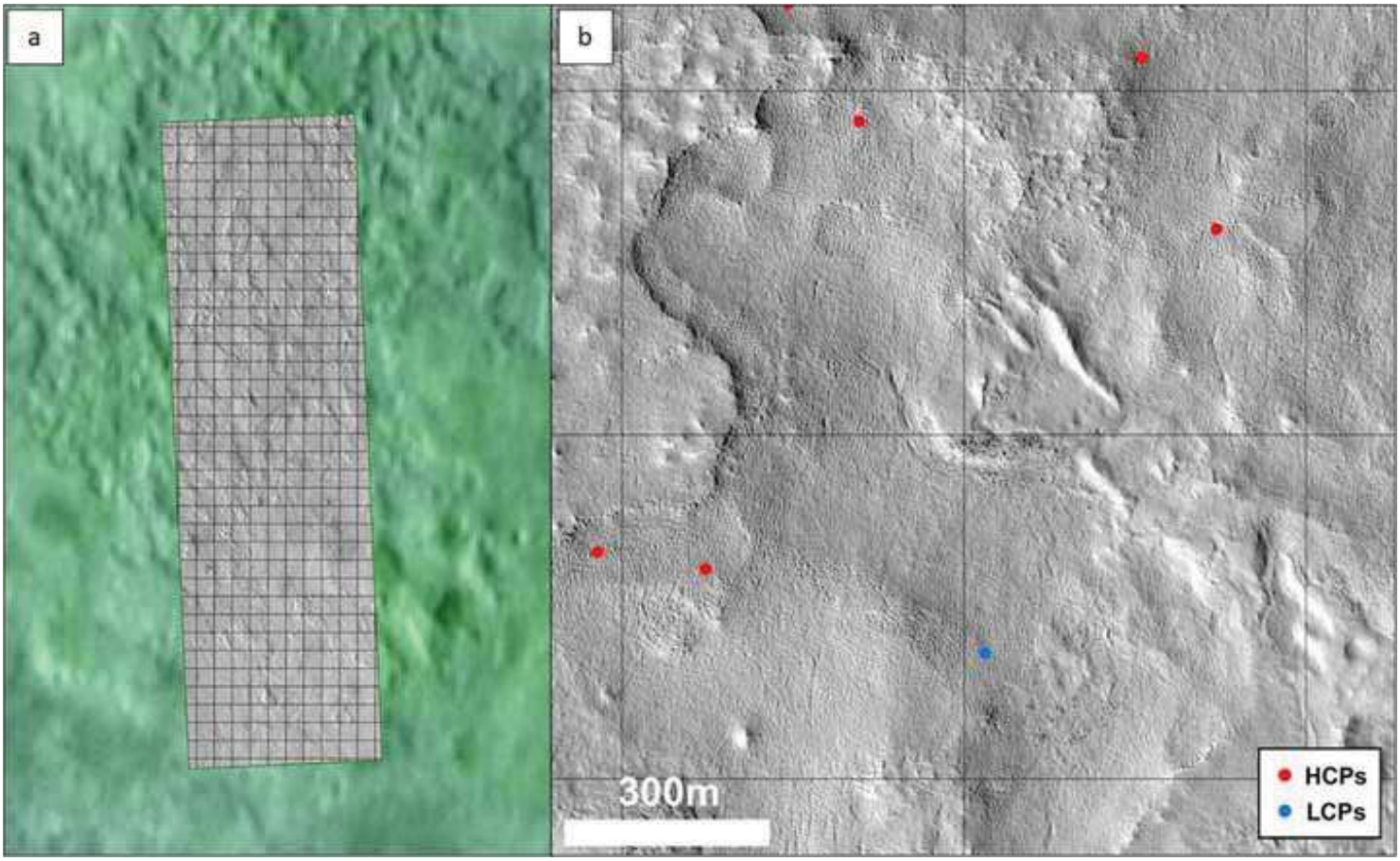

Fig. 3

Click here to access/download;Figure;Fig. 3.tif

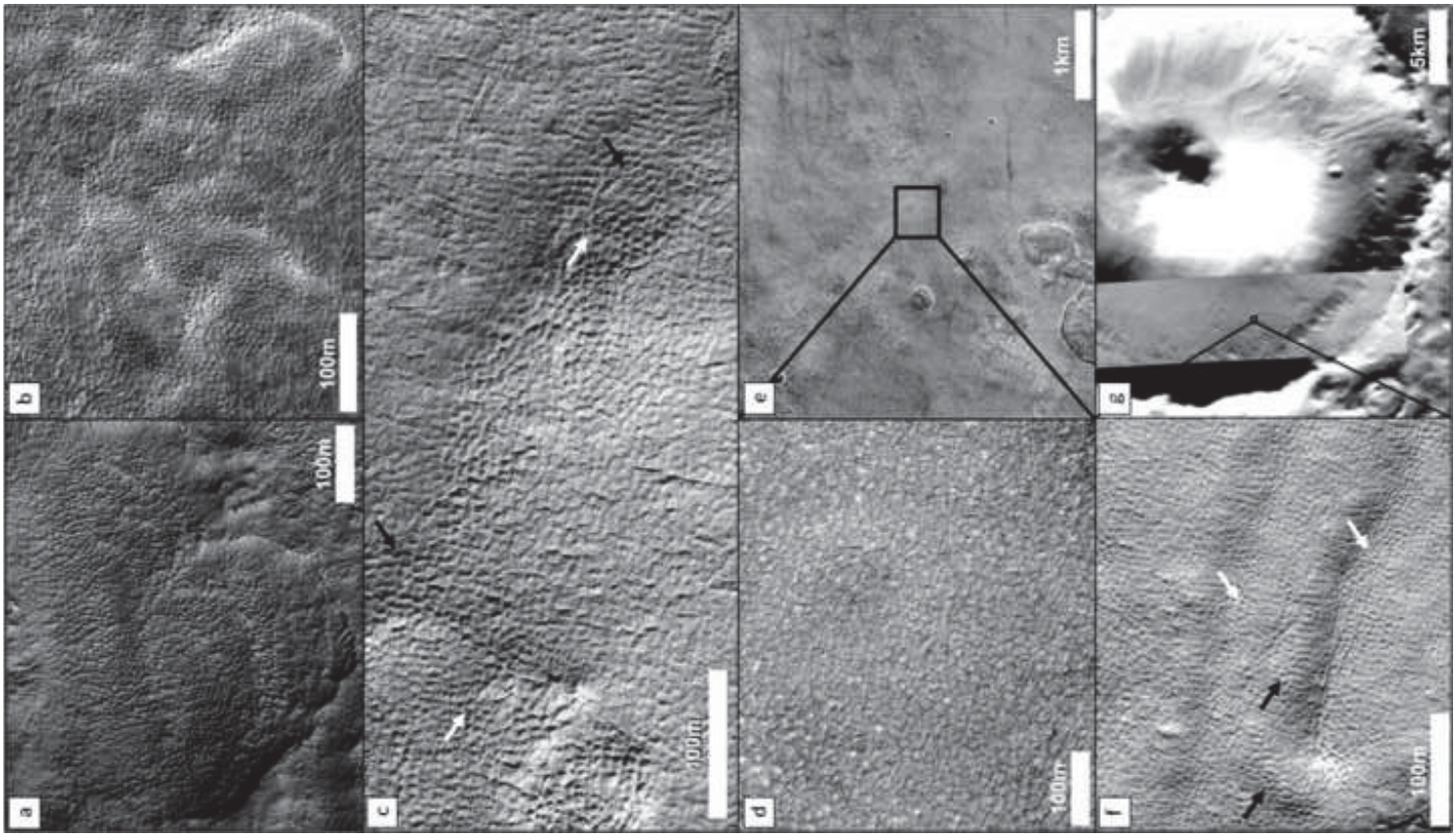

Fig. 4

Click here to access/download;Figure;Fig. 4.tif

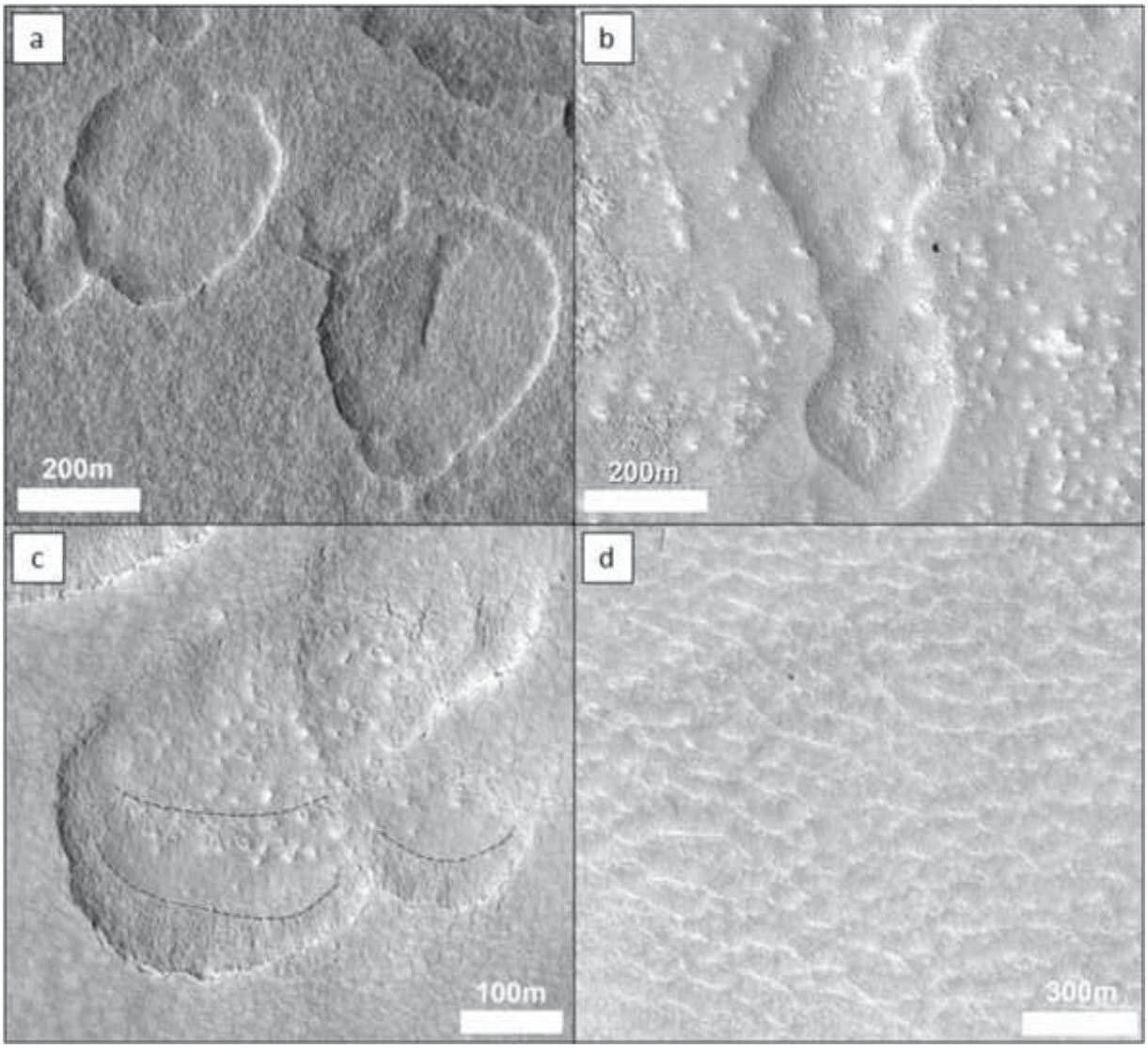

Fig. 5

Click here to access/download;Figure;Fig. 5.jfif

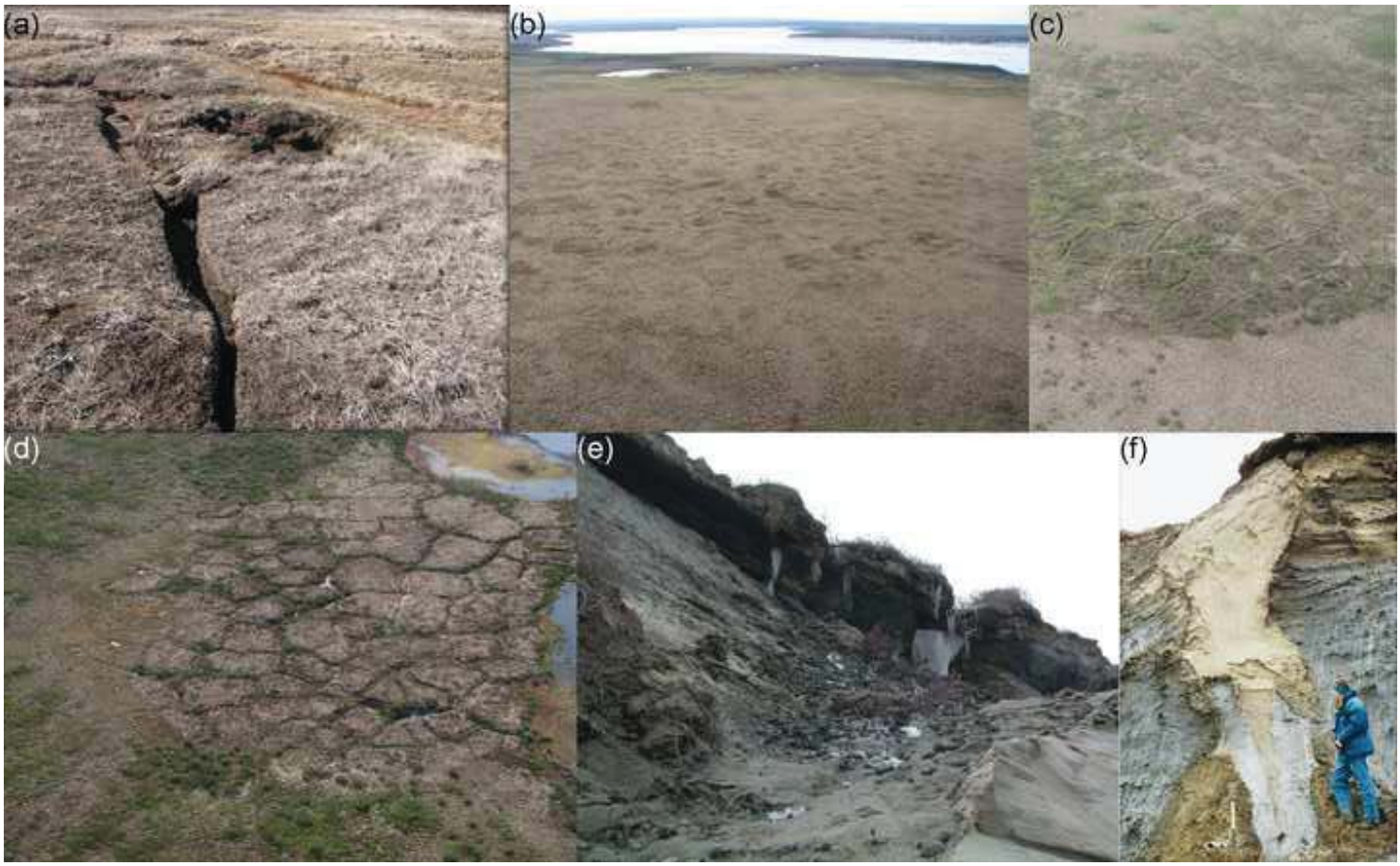

Fig. 6

Click here to access/download;Figure;Fig. 6.bmp

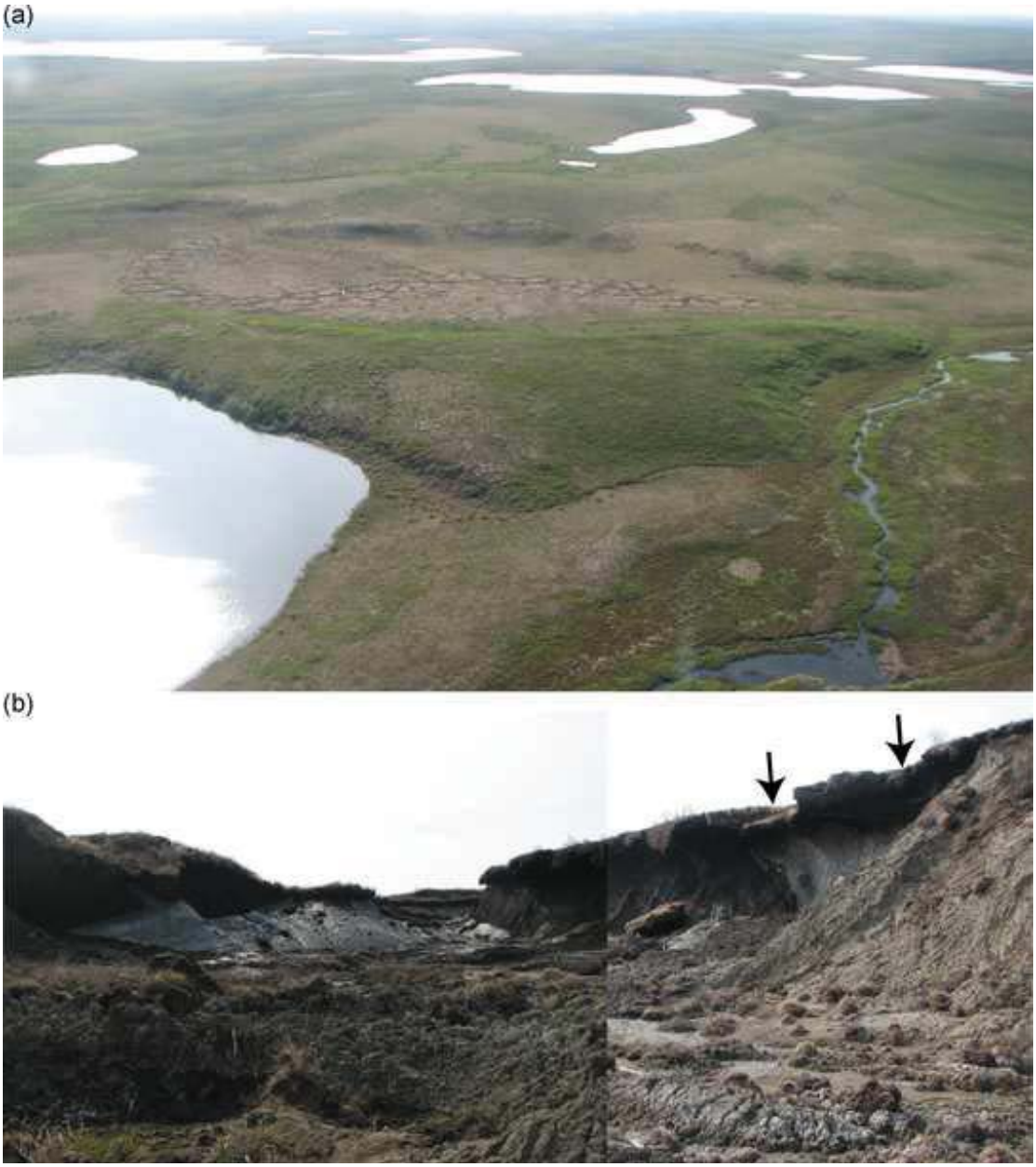

Fig. 7

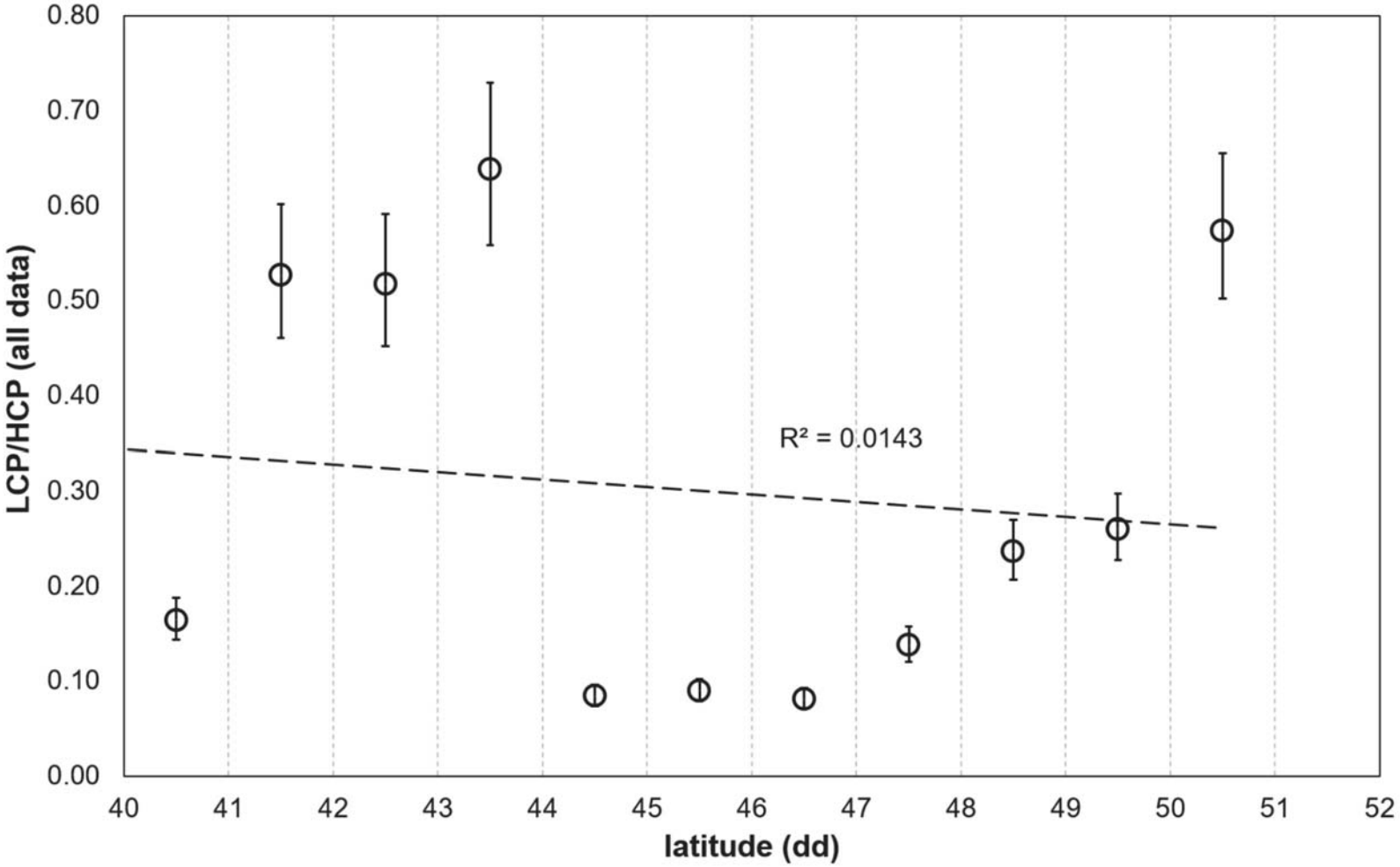
0.80
0.70
0.60
0.50
0.40
0.30
0.20
0.10
0.00
LCP/HCP (all data)
R² = 0.0143
40
41
42
43
44
45
46
47
48
49
50
51
52
latitude (dd)

Fig. 8

Click here to access/download;Figure;Fig. 8.jpg

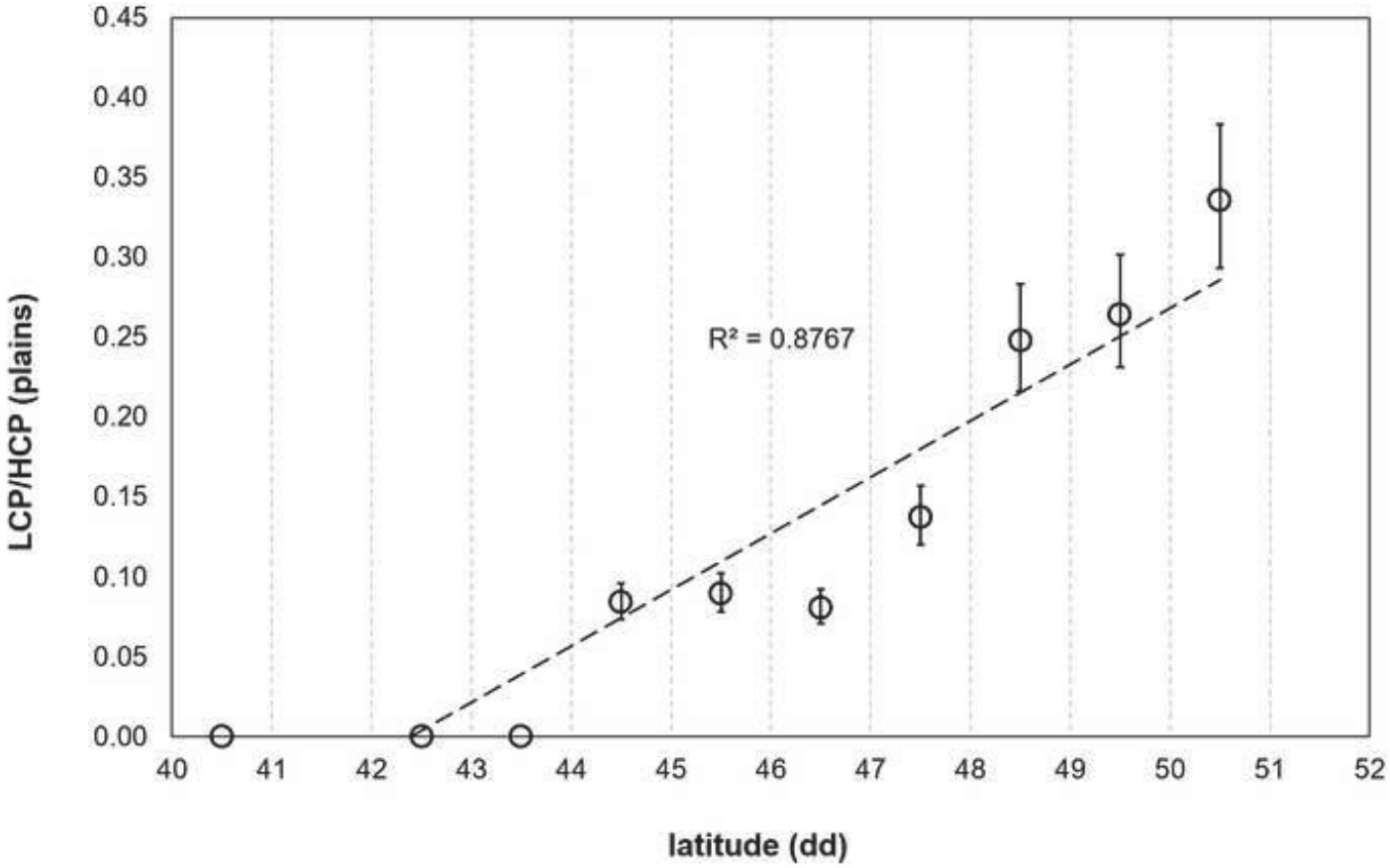

Fig. 9

Click here to access/download;Figure;Fig. 9.tif